Shear-wave splitting in compliant rocks

PETER CARY, XINXIANG LI, GULIA POPOV, and CHANGJUN ZHANG, Sensor Geophysical

Shear-wave splitting is a phenomenon that has received a lot of attention primarily because of its connection with vertically aligned cracks or fractures within reservoirs. However, in most cases the largest amount of shear-wave splitting is observed to occur in the near-surface layers where the rocks are the least consolidated, and so are least likely to be stiff enough to support cracks. Ironically, we have observed during the processing of many multicomponent data sets in western Canada that the largest amounts of shear-wave splitting occur in an area where we least expect to see it—in the highly unconsolidated sediments that comprise the heavy oil plays in the northwestern part of Alberta. At first we thought that the rocks in this area were surely too soft to support cracks and therefore that shear-wave splitting would be smaller than observed elsewhere. The data have taught us that the opposite is true.

Introduction

We show an example in this paper from a 3C-3D survey where the observed shear-wave splitting is large in magnitude and correlates well with known near-surface geography. A change in topography (a 30-m hill on the surface of the 3D survey) appears to be the cause of a large (40 ms) time delay between the fast and slow split shear-wave arrivals observed at the surface. Similarly, on another 3C-3D survey from northern Alberta, Whale et al. (2009) reported an anomalous amount of shear-wave splitting underneath a lake. In another part of the world, there is the well-known example reported by Olofsson et al. (2003) of the correlation of shear-wave splitting with sea-floor subsidence at Valhall Field in the North Sea. On the basis of evidence like this, we argue that the need to connect shear-wave splitting with cracks or fractures has been overemphasized. The observations say that shear-wave splitting is a highly sensitive indicator of nonisotropic changes in local stresses in compliant rocks. An explanation for how shear-wave splitting occurs in rocks that are too compliant to support cracks is required to explain these observations.

Regardless of the explanation for the azimuthal anisotropy, we cannot deny the observations that large amounts of shear-wave splitting occur in highly compliant rocks. Of course we are usually more annoyed by these types of observations than interested in them because the splitting is confined largely to the near-surface layers and has the effect of blurring the image of all deeper layers unless the effects of the splitting are removed. The combination of large shear-wave statics and large shear-wave splitting in the near-surface certainly adds difficulty to the processing of PS data. However, with the correct tools, it is possible to resolve and compensate for these two effects correctly.

Large near-surface shear-wave splitting could be more beneficial than it initially appears if we stop to think about what it can teach us about what to expect from time-lapse seismic in a soft rock environment. Production from reservoirs in the heavy oil plays in northern Alberta is usually stimulated by injection of steam, water, or CO_2. If large amounts of azimuthal anisotropy are observed in near-surface layers in this area because the shear waves in highly compliant rocks are sensitive to nonisotropic stresses, then we would expect time-lapse analysis of the PS data from these areas to show significant differences at the reservoir level due to nonisotropic stresses brought about by fluid injection over time. These changes in shear-wave splitting would be in addition to any overall changes in the P and S velocities caused by changes in the effective stress from the fluid injection. Laboratory measurements have already been made (He and Schmitt, 2006) that indicate that P and S velocities are very sensitive to the effective stress at low effective pressure.

Early 9C-3D time-lapse studies (e.g., Roche et al., 1997; Angerer et al., 2000) have shown anisotropy anomalies that are coincident with large CO_2 concentrations, and appear to be associated with elevated reservoir pressure. 3C-3D surveys have also shown positive correlation between fractures, permeability, and azimuthal anisotropy (e.g., Angerer et al., 2006). However, a lot remains to be learned from time-lapse 3C data, especially in areas where the rocks are as compliant as they are in the heavy oil region of northern Alberta.

As far as we know, the observation of changes in PS data that result from fluid injection have never been observed or reported from the heavy oil area of northern Alberta even though a large amount of multicomponent data have been acquired there. However, this may simply be because no one has ever looked for it. The industry standard in this area is to acquire the data with 3C receivers, but process and interpret only the PP data recorded on the vertical component. The horizontal components that record the PS data are almost always put "on the shelf", waiting for some good reason to be processed because the perception at present is that they do not add significant value.

Shear-wave splitting observations

Our example is from a small (5.6 × 6.4 km) 3C-3D data set acquired over a heavy oil prospect in northern Alberta. These data are from a part of the Western Canadian Sedimentary Basin (WCSB) where you would least expect the rocks to be stiff enough to support cracks or fractures. The Cretaceous sediments in northern Alberta (mostly sands and shales) have average V_P/V_S ratios of about 3. In the near surface, the V_P/V_S ratios are highly variable and can become much higher than 3 (which leads to large shear-wave statics). Although it forms only a small portion of the sedimentary column, the bitumen oil sand in this location is well known for being more like a highly viscous fluid than a solid rock. It has a composition like cold molasses (API gravity of bitumen is around 8°). The older, stiffer sediments in the WCSB have V_P/V_S ratios much closer to 2.

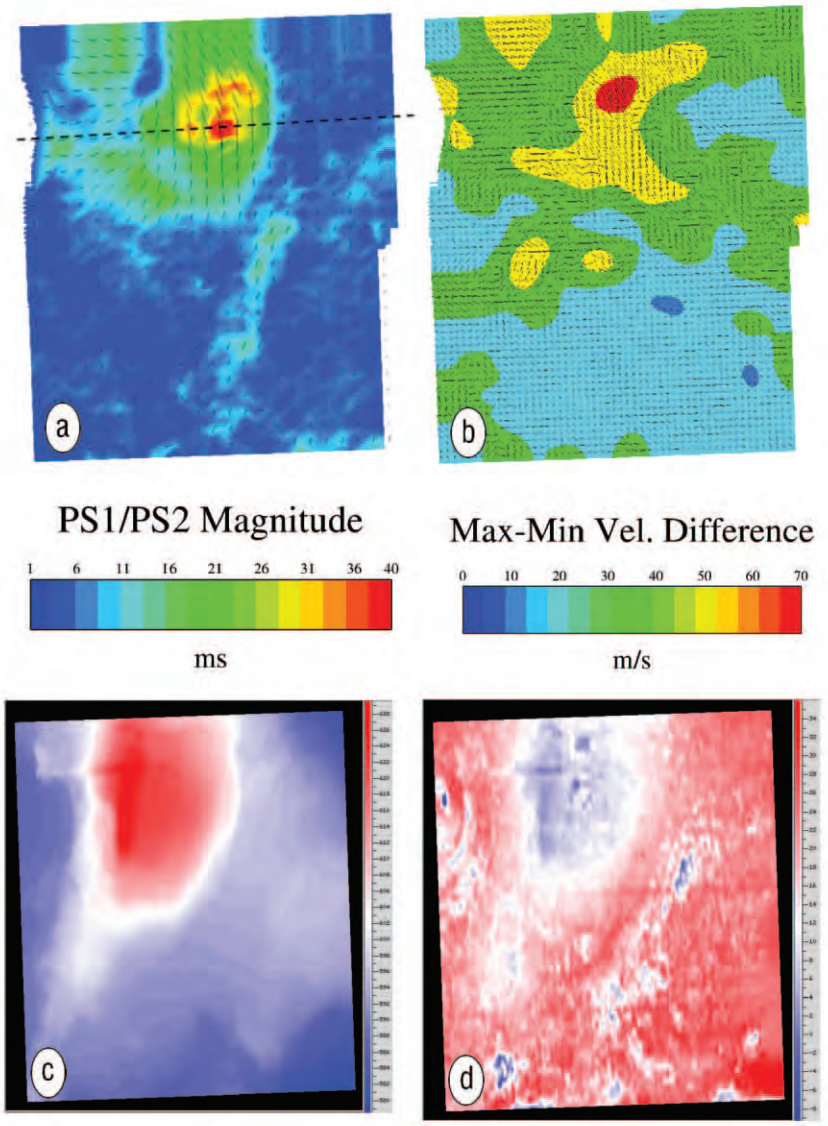

Figure 1. *(a) Shear-wave splitting response of the PS data to near-surface layers. The dashed line indicates the location of the inline shown in Figure 4. (b) Velocity variation with azimuth of shallow PP reflectors. (c) Surface elevation of the 3C-3D survey. The feature in red is a 30-m hill. (d) Refraction statics derived from the PP first-break arrivals showing the impact of elevation changes and Quaternary channels in the near-surface. The PP statics vary by 30 ms over the survey. (e) Shear-wave receiver statics derived from PS reflections. The PS statics vary by 300 ms over the survey.*

Although the data set is small, it illustrates how large the overburden shear-wave splitting effects can be, and how rapidly they can vary, within a small area. Figure 1a shows the results of shear-wave splitting analysis of the azimuthal variations of the PS reflections on the horizontal components (Figure 2). The direction of the needles, which indicates the orientation of the fast S1 axis (the direction of the maximum horizontal stress), varies significantly around the survey. The background color as well as the lengths of the needles denotes the magnitude of the splitting (i.e., the time delay between the fast PS1 arrival and the slow PS2 arrival). There is an obvious "bull's-eye" in the northern part of the survey where the time delay between the fast and slow PS waves reaches as much as 40 ms. It is usually understood that the dominant horizontal stress direction in the WCSB is normal to the Rocky Mountain Deformation Front, which is roughly 45° E of N in this area. We can see that the shorter needles (blue background) do tend toward that direction, but the longer needles generally depart from that direction.

The horizontal transverse isotropy in the near surface that causes the shear-wave splitting observed on the PS data should also cause azimuthal variations in the stacking velocities of the PP data. The simultaneous observation of similar effects on both PP and PS data should increase our confidence in the results. Figure 1b shows the velocity variation with azimuth (VVAZ) results obtained by analyzing azimuthal variations in the stacking velocities of the shallow PP reflections on the vertical component data set (Figure 3). A remarkable similarity exists between the major features of the anisotropy derived from the PP and PS data. The changes in direction as well as the magnitude of the needles in Figures 1a and 1b correspond well with each other, especially over the large bull's-eye. Notice how the needles in both cases turn north-south over the bull's-eye and then turn northwest-southeast to the northwest of the bull's-eye.

These observations from the shallow PP and PS seismic data correlate remarkably well with surface and near-surface geographic features. Figure 1c shows the surface elevations over the 3D survey, Figure 1d shows the receiver refraction statics solution derived from the analysis of the P-wave first-

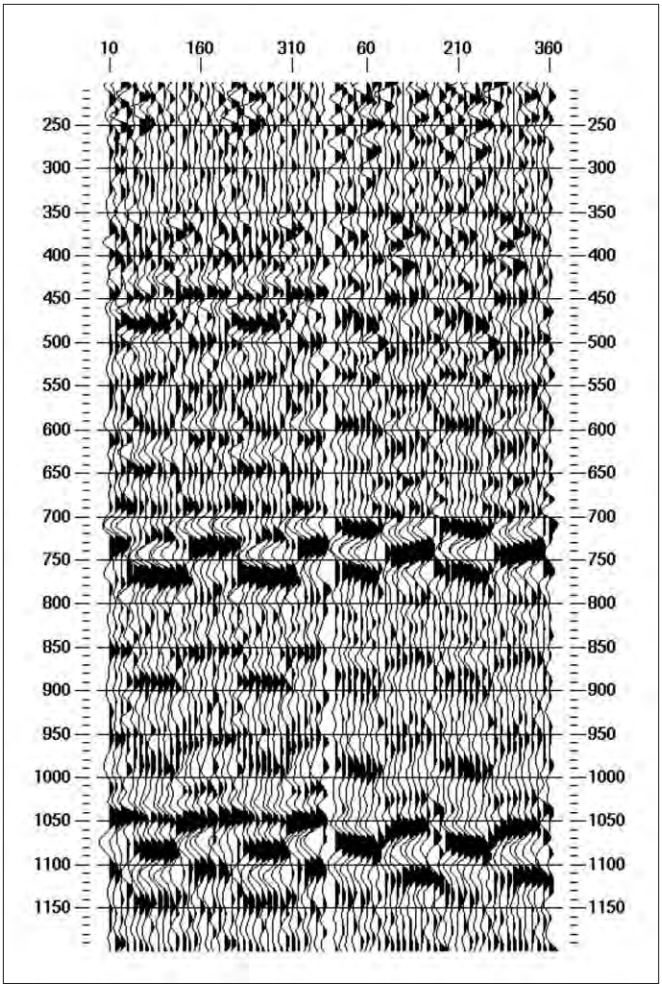

Figure 2. *Limited azimuth stacks near the top of the hill showing the large impact of shear-wave splitting on the PS data. The radial component is on the left and the transverse component is on the right. The horizontal axis is azimuth in degrees.*

break data, and Figure 1e shows the shear-wave receiver statics derived from the PS reflection data.

The elevation map in Figure 1c shows that there is a 30-m hill in the same location as the bull's-eye on the PS and PP azimuthal anisotropy maps in Figures 1a and 1b. The correlation of the hill with the anisotropy anomaly certainly appears to be more than a coincidence. As stated earlier, azimuthal anisotropy is normally explained with the aid of an Earth model that includes vertically aligned cracks or fractures, or some inherent azimuthal difference in the rock fabric. It is not clear which, if any, of these factors is causing the azimuthal anisotropy in this example, but it appears obvious that the hill is somehow involved in generating the large shear-wave splitting and VVAZ anomalies.

As stated earlier, large shear-wave splitting effects in overburden layers have been observed in both land and marine environments around the world. It is unlikely that the overburden could be rigid enough to support cracks or fractures in this area because the sediments are so young and unconsolidated. The hill is probably composed of glacial till. It may be a drumlin and therefore have a flow direction imprinted in the sediments. It may simply be that the hill introduces a load on the surface, and therefore influences the effective stresses in the near-surface layers that the shear waves sense strongly.

If we compare Figure 1a with Figures 1d and 1e, we see that the shear-wave splitting results also show a sensitivity to near-surface Quaternary river channels. The P-wave refraction statics in Figure 1d are influenced by what appears to be a buried river channel going from northeast to southwest across the survey. The shear-wave statics are very strongly influenced by this Quaternary channel as indicated by the diagonal linear feature in blue in Figure 1e. We have observed this correlation of shear-wave splitting with buried channels on many other 3C-3D surveys. Shallow channels can cause large shear-wave statics as well as shear-wave splitting. Notice that the shear-wave statics are very large here. The Quaternary channel causes statics up to 30 ms on the PP data but it causes more than 300 ms of statics on the PS data. In addition to the shear-wave statics, there is about 20 ms of time delay between the PS1 and PS2 arrivals. Since it is easy to confuse the influences of shear-wave statics and shear-wave splitting on PS data, it is important to process the data carefully to distinguish the two effects properly. This usually involves a bootstrap approach where more than one estimation and application of statics and splitting are required, gradually approaching correct and independent solutions for both.

Figure 2 shows a common-azimuth stack of the radial and transverse components of the PS data at a location on the 3D survey near the crest of the hill shown in Figure 1c. The magnitude and the orientation of the shear-wave splitting in Figure 1a are determined by the analysis of this type of data. This display is formed from a gather of horizontal-component traces that have been rotated into radial and transverse components and then sorted by a asymptotic conversion point. The traces then have statics, NMO, and mute applied, are subdivided into 10° azimuth sectors and finally are partially stacked. The azimuth range is from 0 to 360° by 10° increments. The obvious checkerboard pattern on both components is an indication of strong azimuthal anisotropy. The early arrival on the radial component is primarily the PS1 component, and the slow arrival is primarily the PS2 component. The polarity changes on the transverse component whenever the S1 or S2 axis is crossed. So at this location the S1 direction is approximately NS and the time delay is 30–40 ms.

Notice that the shallow PS reflections in Figure 2 are much noisier than the deeper reflections. This is due to the lower fold of traces resulting from larger offsets being muted off at early times. It is the shallow reflectors that we would really like to use for the shear-wave splitting analysis since we believe the strongest anisotropy is near the surface. We are unfortunately forced to use the deeper PS reflections to determine the shallow anisotropy parameters due to the degradation of the signal-to-noise ratio at early times. This situation makes it virtually impossible to convert the maximum measured time delay of 40 ms into an estimate of anisotropy percentage since we do not know with any confidence where most of that time delay is occurring, except that it is above

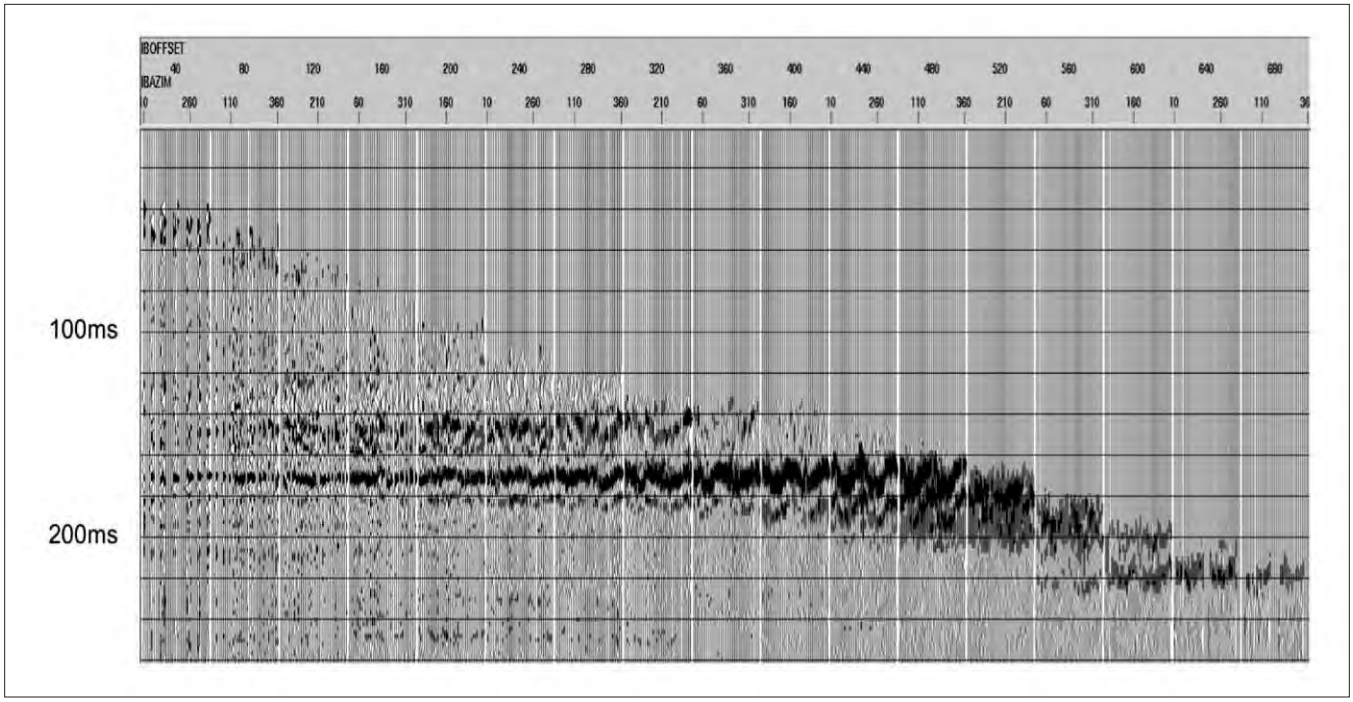

Figure 3. *Common-azimuth, common-offset display of shallow PP reflections near the top of the hill. The offset increases from 40 to 680 m by 40-m increments. Within each 40-m offset range, the azimuth varies from 0 to 360° by 10° increments. The sinusoidal variation of velocity with azimuth of the reflection at 170 ms indicates the influence of azimuthal anisotropy.*

the first strong reflector.

Figure 3 shows a common-offset, common-azimuth display of a group of NMO-corrected traces near the crest of the hill shown in Figure 1c. This display illustrates the effect of the azimuthal anisotropy anomaly that corresponds to the hill on the shallow events in the PP data. This display was formed by applying isotropic NMO, sorting the data into offset bins (from 40 to 680 m by increments of 40 m) and then sorting the data within each azimuth range into azimuth sectors (10–360° by increments of 10°) and partially stacking. The sin 2θ azimuthal variation in arrival time of the large-amplitude event, which grows in amplitude with offset, is what is expected from horizontal transverse isotropy. The NMO velocity of this event is about 1800 m/s and the maximum minus minimum velocity difference (the magnitude of the sin 2θ variation) is about 70 m/s, so velocity varies with azimuth by about 4% for this event.

From the point of view of imaging the deeper PS data, it is not important to know exactly what is causing the shear-wave splitting near the surface; however, it is crucial to remove its effects. We can see from the limited-azimuth stack in Figure 2 that if we stack over all azimuths of the radial component, we will get severely distorted wavelets. Figure 4 shows the radial, and the radial layer-stripped, PS data along one inline which passes through the middle of the large shear-wave splitting anomaly that corresponds to the hill (shown by a dashed line in Figure 1a). Throughout the anomalous zone, the wavelets are strongly distorted on the radial data, and much more uniform on the layer-stripped data. The layer-stripped data have had the overburden splitting effects removed by rotations and static shifts so that the data appear as if acquired with an azimuthally isotropic overburden. We can see how crucial it is to remove the effects of splitting in order to image the PS data properly. In contrast to this large effect on the PS image, the effects of azimuthal anisotropy on the shallow PP data are relatively small, and are confined to the largest offsets on the shallow events (Figure 3). Since the effects of the shallow anisotropy are confined to such large angles in the shallow events, excellent high-resolution PP images for deeper layers were obtained without any special considerations for near-surface azimuthal velocity variations.

Discussion and conclusions

The argument for why shear-wave splitting is sensitive to subsurface pore pressure is that when a shear wave impinges on a layer with vertically aligned cracks or fractures, then the pore pressure in the cracks will be sensitive to nonisotropic stresses because the cracks are the most compliant part of the rock. The cracks or fractures will preferentially open in the orientation normal to the least compressive local effective stress. Shear-wave splitting is sensitive to these changes. Therefore, shear-wave splitting should be a good way to monitor pore pressure changes within a cracked or fractured reservoir. This argument is due to Crampin (1985).

This simple argument has been supported by observations in many experiments, for example in the first time-lapse experiment that was designed to measure changes in shear-wave splitting (Roche et al., 1997; Angerer et al. 2001). However, very early on, it was often observed that the largest effects of shear-wave splitting occur in the near-surface layers well above reservoir levels. This is true both on land (e.g., Lynn, 1991; Winterstein and Meadows, 2001) and in

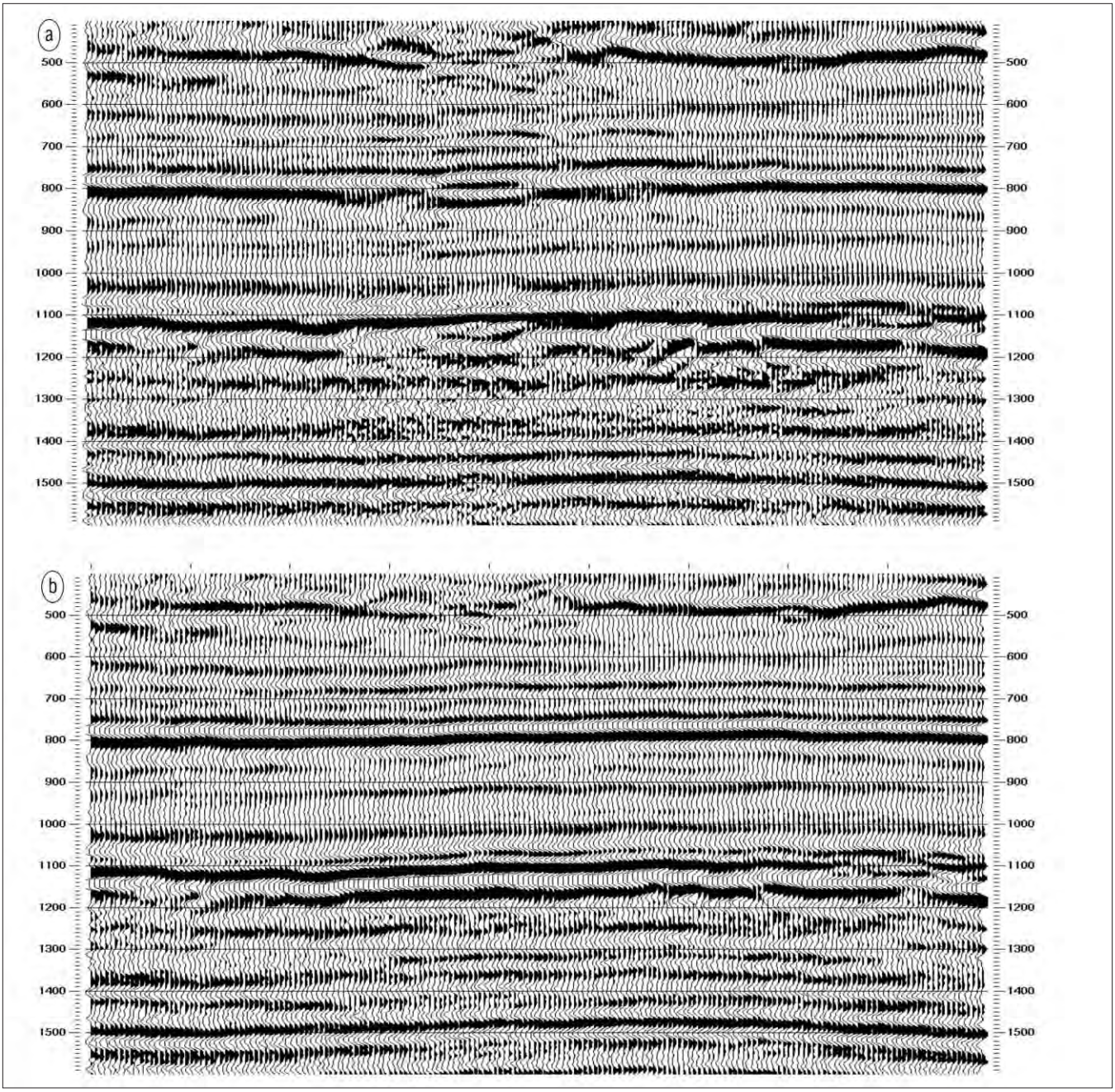

Figure 4. *(a) An inline of the radial component stack though the hill (indicated by the dashed line in Figure 1a). The distortion of the wavelet near the middle of the line at 800 ms, and elsewhere, is due to shear-wave splitting. (b) The same inline of the radial layer-stripped stack, with the near-surface splitting effects removed. The reflection at 800 ms, and elsewhere, is much more coherent and consistent.*

the marine environment (Oloffsson et al. 2003; Gumble and Gaiser, 2006). Typically, these shallow layers have young, unconsolidated sediments so it is not obvious that the shear-wave splitting could be caused by cracks. It is easy to understand why there should be a lot of pore space between the grains in these near-surface layers, but it is much harder to accept that these highly compliant rocks could be strong enough to support cracks or fractures.

Previous observers have also questioned the necessity of invoking cracks as a means of explaining how shear-wave splitting is generated. In their discussion of the shear-wave splitting observations at the Teal South project in the Gulf of Mexico, Gumble and Gaiser say that "S-wave anisotropy may be caused also by horizontal stresses, particularly in the near surface, which may not be related to through-going fractures." Also Oloffsson et al., in their compelling example of the correlation of shear-wave splitting with the seabed subsidence bowl at Valhall Field in the North Sea, attribute the circular anisotropy pattern observed in the shallowest layers to lateral stresses, with no mention of cracks.

Our intention in this article is not to discredit in any way the argument that links shear-wave splitting with cracks or fractures. We simply want to point out that a broader explanation may be required to explain the many observa-

tions that suggest that the more compliant a medium is, the more sensitive it is to shear-wave splitting due to nonisotropic stresses.

Ideally we would like to get the maximum benefit from multicomponent data by combining our understanding from the joint recording, processing and interpretation of all the components of multicomponent data sets together. Toward this end, our land 3C-3D example has shown how near-surface layers which exhibit strong horizontal transverse isotropy cause both azimuthal variations in the stacking velocities of the P-wave data and shear-wave splitting on converted-wave (PS) data. These similarities of how P-waves and S-waves are affected by the subsurface increase our confidence in our interpretation of the subsurface. TLE

References

Angerer, E., S. Crampin, X.-Y. Li, and T. L. Davis, 2000, Time-lapse seismic changes in a CO_2 injection process in a fractured reservoir: 70th Annual International Meeting, SEG, Expanded Abstracts, 1532–1535.

Angerer, E., J. Holden, N. Jones, Y. Freudenreich, E. Maili, and T.-W. Lo, 2006, Getting the whole picture: wide-azimuth multicomponent seismic: The Leading Edge, **25**, no. 9, 1052–1058, doi:10.1190/1.2349808.

Crampin, S., 1985, Evaluation of anisotropy by shear-wave splitting: Geophysics, **50**, no. 1, 142–152, doi:10.1190/1.1441824.

Gumble, J. E., and J. E. Gaiser, 2006, Characterization of layered anisotropic media from prestack PS-wave-reflection data: Geophysics, **71**, no. 5, D171–D182, doi:10.1190/1.2335419.

He, T. and D. Schmitt, 2006, P- and S-wave velocity measurements and pressure sensitivity analysis of AVA response: CSEG Expanded Abstracts, 398–404.

Lynn, H., 1991, Field measurements of azimuthal anisotropy: First 60 meters, San Francisco Bay area, CA, and estimation of the horizontal stresses' ratio from Vs1/Vs2: Geophysics, **56**, no. 6, 822–832, doi:10.1190/1.1443100.

Olofsson, B., T. Probert, J. H. Kommedal, and O. I. Barkved, 2003, Azimuthal anisotropy from the Valhall 4C/3D survey: The Leading Edge, 22, no. 12, 1228–1235, doi:10.1190/1.1641375.

Roche, S. L., T. L. Davis, and R. D. Benson, 1997, 4D/3C seismic study at Vacuum Field, New Mexico: 67th Annual International Meeting, SEG, Expanded Abstracts, 886–889.

Whale, R., R. Bale, K. Poplavskii, K. Douglas, X. Li, and C. Slind, 2009, Estimating and compensating for anisotropy observed in PS data for a heavy oil reservoir: 79th Annual International Meeting, SEG, Expanded Abstracts, 1212–1216.

Winterstein, D., G. S. De, and M. A. Meadows, 2001, Twelve years of vertical birefringence in nine-component VSP data: Geophysics, **66**, no. 2, 582–597, doi:10.1190/1.1444950.

Corresponding author: peter_cary@sensorgeo.com